CCDC134 serves a crucial role in embryonic development

BIAOYI YU[1,2*], TIANZHUO ZHANG[1,2*], PENG XIA[1,2], XIAOTING GONG[1,2],
XIAOYAN QIU[1,2] and JING HUANG[1-3]

[1]Department of Immunology, School of Basic Medical Sciences, Peking University Health Science Center;
[2]Key Laboratory of Medical Immunology, Ministry of Health;
[3]Peking University Center for Human Disease Genomics, Beijing 100191, P.R. China

Abstract. Coiled-coil domain containing 134 (CCDC134), a characterized secreted protein, may serve as an immune cytokine and illustrates its potent antitumor effects by augmenting CD8^{+} T-cell-mediated immunity. Additionally, CCDC134 may also act as a novel regulator of human alteration/deficiency in activation 2a, and be involved in the p300-CBP-associated factor complex and affect its acetyltransferase activity. To clarify the biological and pathological function of CCDC134, the present study generated a viable and fertile *Ccdc134$^{fl/fl}$* mouse strain that allowed temporal and spatial control of gene ablation. *Ccdc134$^{-/-}$* embryos generated by crossing of *Ccdc134$^{fl/fl}$* mice with human β-actin-Cre or zona pellucida 3-Cre transgenic mice were embryonic lethal from embryonic day (E)12.5 to birth. *Ccdc134* loss was associated with severe hemorrhages in the brain ventricular space and neural tube, pale and abnormal livers, cardiac hypertrophy and placental distress. Furthermore, it was demonstrated that a fraction of E13.5 fetal livers and brains exhibited reduced cell proliferation and vascular endothelial cell defects. CCDC134 also exhibited a dynamic and specific expression pattern during embryo development. The present results suggest that *Ccdc134* may have specific biological functions in regulating mouse embryonic development.

Correspondence to: Professor Jing Huang, Peking University Center for Human Disease Genomics, 38 Xue-yuan Road, Beijing 100191, P.R. China
E-mail: huangjing82@bjmu.edu.cn

*Contributed equally

Introduction

Coiled-coil domain containing 134 (CCDC134) was first identified through high-throughput functional screening systems using an Elk1 trans-reporting system in the Peking University Center for Human Disease Genomics (Beijing, China). Our earlier study demonstrated that CCDC134 is a classical secreted protein that inhibited Elk1 transcriptional regulation and mitogen-activated protein kinase (MAPK) signal transduction through the Raf-1/MEK/extracellular signal-regulated kinase and c-Jun N-terminal kinase/stress-activated protein kinase pathways (1). A previous study also identified a role for CCDC134 in tumor development; CCDC134 was identified as a candidate biomarker of malignant transformation with decreased expression in gastric cancer, and targeted small interfering RNA knockdown of CCDC134 promoted tumor migration and invasion via the MAPK pathway (2).

CCDC134 was proposed to have immune cytokine function, and directly promoted CD8^{+} T-cell activation, proliferation and cytotoxicity (3). Additionally, CCDC134 demonstrated its potent antitumor effects by augmenting CD8^{+} T-cell-mediated immunity (3). Mechanistically, exposure to CCDC134 promoted CD8^{+} T-cell proliferation through the Janus kinase 3-signal transducer and activator of transcription 5 pathway, and two members of the γ_c cytokine family could effectively block CCDC134 binding to activated CD8^{+} T-cells, which provided evidence that CCDC134 may serve as a potential member of the γ_c cytokine family (3).

On the basis of CCDC134 molecular structure and transcription regulatory capacity, it is suggested that CCDC134 is also a nuclear protein that acts as a critical regulator of human alteration/deficiency in activation 2a (hADA2a) to enhance the stability of hADA2a and inhibit its proteasome-dependent degradation (4). Additionally, CCDC134 participated in the p300-CBP-associated factor (PCAF) complex via hADA2a to affect its histone acetyltransferase (HAT) activity, which primarily acetylated lysine 14 of H3, but also less efficiently acetylated lysine 8 of H4 (5). Also, CCDC134 was involved in the repair of ultraviolet-induced DNA damage (4). The above evidence indicates that CCDC134 may function as a cytokine that mediates immune responses and a nuclear protein, similar to high mobility group box chromosomal protein 1, interleukin-1α (IL-1α) and IL-33 (6,7).

Thus, CCDC134 may serve as a multi-faceted adaptor/scaffolding protein to relay cellular signals to the cytoplasm and the nucleus. To determine if any of these cellular mechanisms for CCDC134 may be biologically relevant and significant *in vivo*, the present study generated a murine model carrying a conditional allele for *Ccdc134*. The present study reports the generation and first characterization of a germline *Ccdc134* null mutant allele in mice, which, when homozygous, is embryonic lethal and may impair embryonic angiogenesis.

Materials and methods

Targeting the Ccdc134 allele. The *Ccdc134* targeting vector was generated with two flippase recognition target (FRT) sites flanked by a neomycin (neo)-resistant cassette upstream of the existing 3' loxP site, and the 5' loxP site was inserted into upstream exon 3, by Nanjing Biomedical Research Institute of Nanjing University (Nanjing, China), according to well-described principles and methods (8). The targeting region of the recombination vector and its relation with the *Ccdc134* locus are demonstrated in Fig. 1A. The targeting vector was linearized with *Not*I (New England BioLabs, Inc., Ipswich, MA, USA) and electroporated into B6/BLU embryonic stem (ES) cells. G418-resistant clones were screened for homologous recombination by long range polymerase chain reaction (PCR). Out of 64 clones, 4 were further identified with correct targeting by Southern blot analysis.

Subsequently, injection of two targeted ES cells into B6 recipient blastocysts (obtained from C57BL/6 female mice) produced 2 male and 2 female chimeras that, on crossing with B6 mice (6-8-week-old male or female mice; weight, 18-20 g) purchased from Beijing Vital River Laboratory Animal Technology Co., Ltd. (Beijing, China), showed germline transmission. Male chimeras were mated with C57BL/6 females in the ratio of 1:3 to generate the *Ccdc134*$^{fln/+}$ mouse line. Neo cassette was removed by crossing with FLP-expressing transgenic mice to generate a *Ccdc134*$^{fl/+}$ mouse line. *Ccdc134*$^{fl/+}$ mice were intercrossed to generate a *Ccdc134*$^{fl/fl}$ conditional allele line, and maintained as a homozygous stock. *Ccdc134*$^{fl/fl}$ females were bred with human β-actin (ACTB)-Cre or zona pellucida 3 (ZP3)-Cre mice to generate a *Ccdc134*$^{+/-}$ heterozygous knockout (KO) mouse line. Finally, *Ccdc134*$^{+/-}$ mice were intercrossed to generate *Ccdc134*$^{+/+}$, *Ccdc134*$^{+/-}$ and *Ccdc134*$^{-/-}$ embryos used for experiments.

The mice were housed and bred under pathogen-free conditions at the Laboratory Animal Research Facility of Peking University Health Science Center (Beijing, China). A total of 5 mice/cage were maintained under laboratory conditions at 25℃, under a normal 12-h light/dark cycle with a humidity of 55% and access to food and water *ad libitum*. Experimental procedures were approved by the Institutional Animal Care and Use Committee of Peking University Health Science Center (Beijing, China), following the guidelines of the Care and Use of Laboratory Animals.

Genotypic analyses. DNA was extracted from ES cells using a genomic DNA extraction kit (Qiagen China Co., Ltd., Shanghai, China) following the manufacturer's protocol. Screening of ES cells was performed by long range PCR analysis for 3'-end screening using a targeting vector-specific forward primer (5'-GCATCGCATTGTCTGAGTAGGTG-3') and a reverse primer (5'-TCTTGCAGAGCAAGAGCGAG-3') inside the targeted region. In addition, a second pair of primers specific for 5'-end screening outside of the target region was used forward, 5'-AACCTCACCCACTCTCTCACCG-3' and reverse, 5'-AAGGGTTATTGAATATGATCGGA-3'. PCR analysis was performed using a Takara LA Taq long PCR system (Takara Biomedical Technology Co., Ltd., Beijing, China) using conditions as follows: Denaturation at 94℃ for 5 min; followed by 30 cycles of amplification at 94℃ for 1 min, 55℃ for 1 min and 65℃ for 5 min; and a final extension step at 72℃ for 10 min.

High molecular weight genomic DNA was extracted from ES cells, digested with either *Spe*I or *Sac*I (New England BioLabs, Inc.) and subjected to electrophoresis in 0.9% agarose gel. For Southern blot analysis, genomic DNA was transferred to a nylon membrane overnight, and then hybridized overnight at 42℃ using a 5' external probe with *Spe*I-digested DNA or 3' external probe with *Sac*I-digested DNA specific to the *Ccdc134* sequence with ^{32}P (GE Healthcare, Chicago, IL, USA) by a random prime labeling method. Finally, the blot was monitored with radioautograph to confirm homologous recombination.

Genomic DNA from tails of 3-week-old pups or whole embryos was used for genotyping. PCR analysis was performed using a Takara Taq DNA polymerase system (Takara Biomedical Technology Co., Ltd.) using conditions as follows: Denaturation at 94℃ for 5 min; 35 cycles of amplification at 94℃ for 30 sec, 55℃ for 30 sec and 72℃ for 30 sec; and a final extension step at 72℃ for 5 min. Two types of *Ccdc134* PCR primers used for PCR analysis were as follows: p1, 5'-TCCTAACCCTGTCGCTCCCT-3'; p2, 5'-CCAGACAGAGGTGAGCTGCT-3'; p3, 5'-GCACCCCTGAGCCAAGTTTAG-3'; and p4, 5'-CCTAACCTATGCCTCCAAAG-3'. Genomic DNA from the targeted allele yields a 615-bp fragment with a primer pair p1/p3, and a wild-type allele yields a 420-bp fragment with primer pair p2/p3, or a 490-bp fragment with p1/p4.

Quantification of mRNA by reverse transcription-quantitative PCR (RT-qPCR). Total RNA was extracted from *Ccdc134*$^{+/+}$, *Ccdc134*$^{+/-}$ and *Ccdc134*$^{-/-}$ embryos at different stages with TRIzol reagent (Invitrogen; Thermo Fisher Scientific, Inc., Waltham, MA, USA), following the manufacturer's protocol. cDNA was synthesized using a Revert Aid First Strand cDNA synthesis kit (Fermentas; Thermo Fisher Scientific, Inc., Pittsburgh, PA, USA), following the manufacturer's recommendations. The following PCR cycling conditions were used: Denaturation at 94℃ for 3 min; 35 cycles of amplification at 94℃ for 30 sec, 55℃ for 30 sec and 72℃ for 30 sec; and a final extension step at 72℃ for 5 min. *Ccdc134* primer sequences used for RT were as follows F1, 5'-GTTGGCACTGAAGAACCTGG-3' and R1, 5'-ACGGGTTCCGGAAGTCAGAA-3'. The qPCR analysis using SYBR-Green master mix was performed using an ABI 7500 Real-Time PCR system (both from Applied Biosystems; Thermo Fisher Scientific, Inc., Waltham, MA, USA) according to the manufacturer's protocol (9). The following primer sequences were used: *Ccdc134* forward, 5'-GCTCCCTTCTCCCTGCAC-3' and reverse, 5'-AGGCCACAGGAGGACAGA-3'; and glyceraldehyde 3-phosphate dehydrogenase (*GAPDH*) forward, 5'-AAGAGGGATGCTGCCCTTAC-3' and reverse, 5'-CCATTTTGTCTACGGGACGA-3'. The mRNA expression levels of
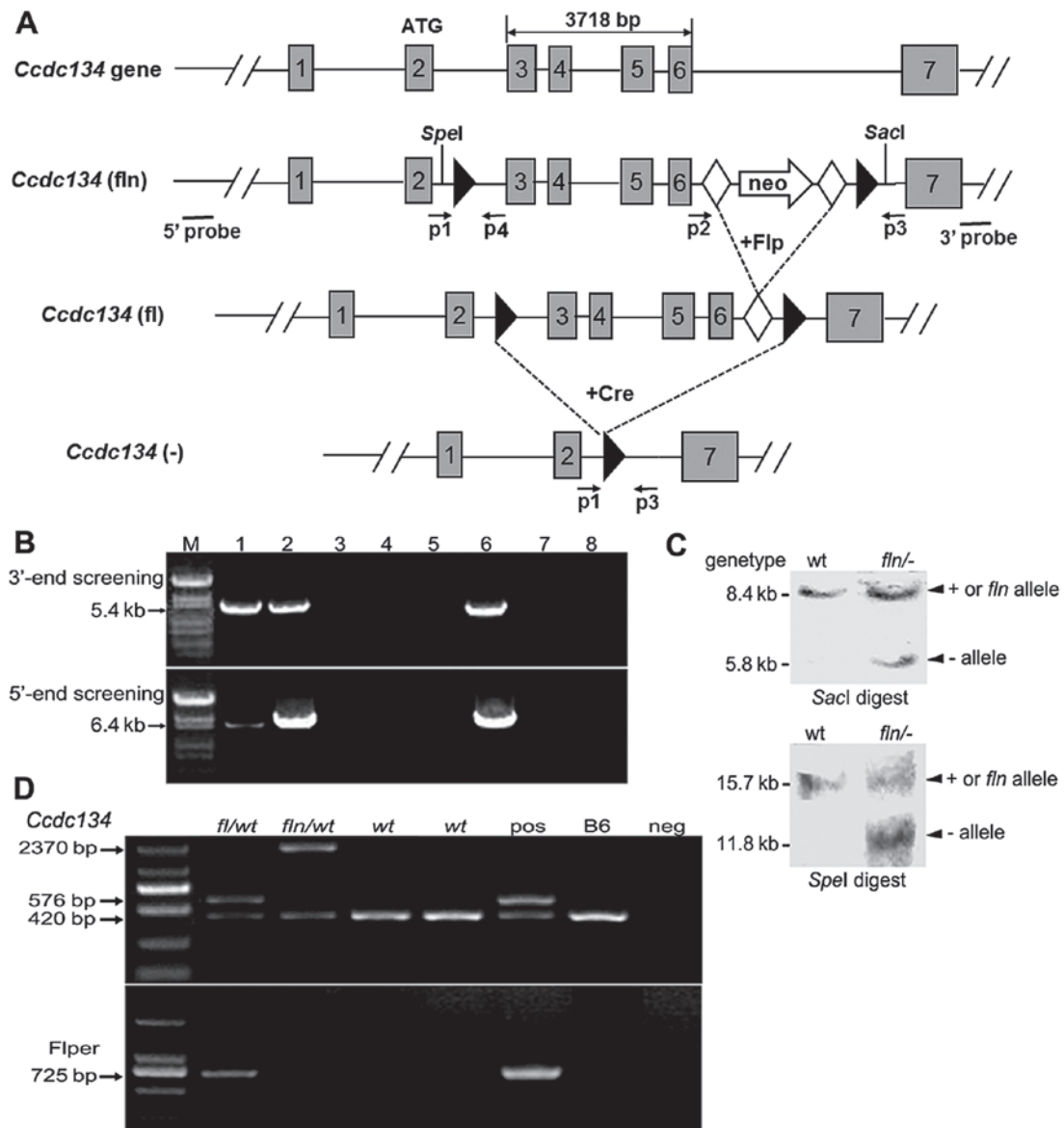
Figure 1. Conditional targeting strategy and screening for homologous recombination of the *Ccdc134* gene. (A) Schematic diagram of the *Ccdc134* gene targeting strategy and gene deletion in mutant mice. The targeting construct was made by inserting a neo resistance gene flanked by flippase recognition target sites (closed diamond) between exon 6 and 7. LoxP sites (closed triangles) were placed flanking exon 3-6. The neo cassette was excised by crossing with FLP-expressing transgenic mice to generate the floxed allele. 5' and 3' probes outside the homologous region were used for Southern blot analysis. (B) Examples of PCR screening assays of neo-resistant clones (lanes 1-5) following transfection of linearized targeting construct and drug selection. Each clone was amplified separately for the recombinant allele (5.4 and 6.4 kb, as predicted) using specific primers for 3'-and 5'-end screening by long range PCR. Here, clones 1 and 2 (lanes 1 and 2) were identified as positive. In the agarose gel: Lane 1-5, amplification using DNA template from clone 1-5; lane 6, positive control; lane 7, control mouse DNA; lane 8, control mix, no DNA. (C) Representative Southern blot analysis used to confirm correct targeting. DNA was digested with either *Spe*I or *Sac*I restriction enzymes and the 5' or 3' probe was used to detect wt, fln and - alleles at the expected size: wt allele, 15.7 (*Spe*I) or 8.4 kb (*Sac*I); and fln, 11.8 (*Spe*I) or 5.8 kb (*Sac*I). (D) A representative gel image of the PCR products. The wt and targeted alleles without neo produce products of 420 and 576 bp, respectively. Also, *fl/wt* was found to lack neo but contain FLP to produce a 725-bp fragment, whereas the PCR product of *fln/wt* should be 2,370 bp. *Ccdc134*, coiled-coil domain containing 134; FLP, flippase in the recombinant embryonic stem cells; neo, neomycin; PCR, polymerase chain reaction; wt, wild-type; fl, floxed; fln, floxed allele with neomycin cassette; +, wild-type; -, null; pos, positive control; neg, negative control; M, marker.

Ccdc134 were normalized to *GAPDH*. All samples were assayed in duplicate, and average values were used for quantification (9).

Western blot analysis. Whole embryos were homogenized with a Dounce glass homogenizer (Kimble Glass, Inc., Deerfield, IL, USA) in radioimmunoprecipitation assay lysis buffer containing fresh protease inhibitor cocktail (Roche Applied Science, Penzberg, Germany). Protein concentrations were determined using a BCA Protein assay kit (Pierce; Thermo Fisher Scientific, Inc., Rockford, IL, USA). The

cell lysates (100 μg) were separated by 12.5% SDS-PAGE, transferred to a nitrocellulose membrane and blocked with 5% non-fat milk for 1 h at room temperature. The membrane was probed with rabbit anti-CCDC134 polyclonal antibody (1:500; sc-86363; Santa Cruz Biotechnology, Inc., Dallas, TX, USA) and mouse anti-β-actin monoclonal antibody (1:1,000; TA09; OriGene Technologies, Inc., Beijing, China) at 4°C overnight. Subsequently, the membrane was incubated at room temperature for 1 h using DyLight 780-conjugated secondary antibodies (1:5,000; 53064; Thermo Fisher Scientific, Inc.,

Waltham, MA, USA). The protein bands were visualized and an infrared fluorescence image was obtained using an Odyssey infrared imaging system (LI-COR Biosciences, Lincoln, NE, USA).

Histology and immunohistochemistry analysis. Whole embryos at 13.5 days post coitus (E13.5) were fixed in 10% formaldehyde solution at room temperature for over 24 h, embedded in paraffin, sectioned at 5-μm thickness, stained with hematoxylin for 4 min, and stained with eosin for 2 min. All procedures were performed at room temperature for histologic examination. Images were captured on a BX-53 inverted fluorescence microscope (Olympus Corp., Tokyo, Japan) at different magnifications (x2, x10 and x20), and processed with Adobe Photoshop CS 5.0 (Adobe, San Jose, CA, USA).

For immunohistochemistry staining, slides were deparaffinized, hydrated, and boiled in a steamer for 3 min in 0.01 M sodium citrate buffer for antigen retrieval. Sections were first treated with 3% H_2O_2 at room temperature to quench endogenous peroxidase, washed several times with phosphate-buffered saline (PBS) (pH 7.2), blocked with 10% normal goat or rabbit serum (OriGene Technologies, Inc.) at 37°C for 1 h, and then incubated with primary antibodies at 4°C overnight. The following antibodies were used: Rabbit anti-CCDC134 (1:100; sc-86363; Santa Cruz Biotechnology, Inc.), rabbit anti-vascular endothelial growth factor receptor-2 (Vegfr-2; 1:100; ab2349; Abcam, Cambridge, UK), biotin-labeled anti-Ter119 (1:100; 13-5921-81; eBioscience; Thermo Fisher Scientific, Inc., Waltham, MA, USA), and anti-Ki-67 (1:50; ab16667). After thorough washing, a GTVision™ III detection system/Mo&Rb HRP (GK500705; GeneTech Co., Ltd., Shanghai, China) was applied directly for 30 min at room temperature. After rinsing in PBS, all sections were visualized with 0.05% 3,3'-diaminobenzidine. The sections were then counterstained with hematoxylin at room temperature for 4 min. To quantify proliferating cells, total numbers of Ki-67^{+} nuclei were counted and data presented as Ki-67^{+} nuclei/mm². Fetal brains were stained for Vegfr-2 expression to quantify the vascular density. Images were captured on a BX-53 inverted fluorescence microscope (Olympus Corp.) at different magnifications (x2, x10 and x20), and processed with Adobe Photoshop CS 5.0 (Adobe).

Statistical analysis. All data were expressed as the mean ± standard deviation. The differences among groups were analyzed using one-way analysis of variance followed by Bonferroni correction. Statistical analyses were performed using SPSS 11.0 (SPSS, Inc., Chicago, IL, USA). P<0.05 was considered to indicate a statistically significant difference.

Results

Generation of floxed Ccdc134 allele and mice. To investigate further the biological role of *Ccdc134 in vivo*, the present study attempted to generate conditional *Ccdc134*-null mice using a Cre/loxP strategy. A homologous targeting construct was prepared with the two loxP sites flanking *Ccdc134* exon 3-6, as well as a neo resistance cassette (a positive selection marker) within intron 6, flanked by FRT sites (Fig. 1A). Upon transfection of ES cells with the linearized targeting vector and G418

selection, 64 independent drug-resistant clones were selected and screened for homologous recombination by long range PCR analyses. The 5.4-kb fragment was amplified from the targeted allelic genomic DNA with a primer pair for 3'-end screening, whereas the 6.4-kb fragment was amplified with a primer pair for 5'-end screening (Fig. 1B). A total of 17 clones were identified as potentially homologous targeted lines. Additionally, 4 correctly targeted clones were identified by Southern blot analysis (Fig. 1C).

To generate chimeras, two ES cell lines were injected into blastocysts of C57BL/6J mice. Male offspring with a high degree of chimerism were crossed with C57BL/6J females to generate floxed *Ccdc134* mice (*Ccdc134*[fln/wt]). The neo locus was then removed by crossing with FLP-expressing transgenic mice (10,11). *Ccdc134* conditional allele mice (*Ccdc134*^{fl/fl}) were then generated by intercrossing *Ccdc134*[fl/wt] mice, and their genotyping was performed by PCR analyses using tail-derived DNA (Fig. 1D). The transmission of Ccdc134[wt/wt], *Ccdc134*[fl/wt] and *Ccdc134*^{fl/fl} followed a Mendelian ratio, and homozygous flox mice exhibited wild-type characteristics with normal CCDC134 expression, reproductive capability and lifespan (data not shown), suggesting that the flox alleles do not influence *Ccdc134* gene activity.

Ccdc134 deficiency is embryonically lethal. The *Ccdc134*^{fl/fl} mice were crossed with ACTB-Cre transgenics, which expressed Cre recombinase under the control of the ACTB gene promoter in all cells of the embryo by the blastocyst stage of development, to generate *Ccdc134* constitutive KOs, referred to as *ACTB-Cre-Ccdc134*^{-/-} (Fig. 1A) (12). Genotyping of progeny from intercrossed *Ccdc134* heterozygote (*ACTB-Cre-Ccdc134*^{+/-}) demonstrated that, among 284 pups born, 185 (65%) were heterozygous for a null allele and 99 (35%) were wild-type (*Ccdc134*^{+/+}). No homozygous mice were born, while heterozygous mice were present at the expected Mendelian ratio (Table I). Subsequently, another Cre line, the Zp3-Cre transgenic line, was used in an attempt to delete *Ccdc134* at an earlier stage in embryonic development. Unlike ACTB, Zp3 is expressed in the growing oocyte prior to the completion of the first meiotic division (13). The *Ccdc134* heterozygotes (*Zp3-Cre-Ccdc134*^{+/-}) were generated by crossing female *Zp3-Cre-Ccdc134*[fl/wt] mice with male wild-type. Crosses between these heterozygous mice also delivered only heterozygous (128) or wild-type (64) live pups in the ratio of 2:1, consistent with prenatal lethality of *ACTB-Cre-Ccdc134*^{-/-} embryos (Table I). A representative genotype is demonstrated in Fig. 2A. The complete absence of *Ccdc134* homozygous KO mice is a statistically significant deviation from the expected ratio (P<0.0001; data not shown), suggesting that a homozygous *Ccdc134*-null genotype is embryonically lethal. Timed mating indicated that mortality of *Ccdc134*^{-/-} embryos began between E11.5 and E12.5. The rate of mortality of *Ccdc134*^{-/-} embryos increased after E11.5 (0% until E11.5, 16.67% at E12.5, 42.86% at E13.5 and 100% at E14.5) and mortality was observed in all *Ccdc134*^{-/-} mice at E14.5 (Table I). These data indicate that *Ccdc134* deficiency causes embryonic lethality, supporting a crucial role for *Ccdc134* during embryogenesis.

To confirm the inability of the targeted *Ccdc134* allele to support CCDC134 expression, the wild-type, heterozygous and KO mice embryos at E13.5 were prepared and analyzed

Table I. Genotypes of embryos from timed pregnancies.

Stage	Total	Embryos in each genotype, n		
		Ccdc134^{+/+}	*Ccdc134*^{+/-}	*Ccdc134*^{-/-}
Weaning (human β-actin-Cre)	284	99	185	0
Weaning (zona pellucida 3-Cre)	192	64	128	0
E14.5	33	10	18	5 (5)
E13.5	54	13	27	14 (6)
E12.5	39	8	25	6 (1)
E11.5	32	10	17	5

Numbers in parentheses represent number of mortalities of genotyped embryos. *Ccdc134*, coiled-coil domain containing 134.

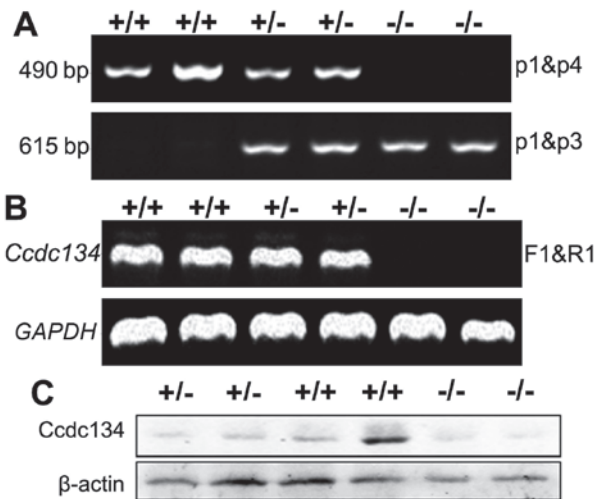Figure 2. Analysis of CCDC134 expression levels in *Ccdc134*^{+/+}, *Ccdc134*^{+/-} and *Ccdc134*^{-/-} mouse embryos. (A) PCR analysis was performed with two primer pairs of p1/p4 and p1/p3. Genomic DNA from the wild-type allele yielded a 490-bp fragment with primer pair p1/p4, and that from the targeted allele yielded a 615-bp fragment with primer pair p1/p3. (B) RT-PCR of total RNA consistently revealed essentially undetectable levels of *Ccdc134* mRNA transcript in *Ccdc134*^{-/-} embryos using primer pairs. (C) Western blot analysis was performed on total cellular lysates obtained from limbs of embryos with the indicated genotypes using specific rabbit anti-CCDC134 antibody. F, forward; R, reverse; CCDC134, coiled-coil domain containing 134.

by RT-PCR and western blot analysis. *Ccdc134* mRNA were not detected in *Ccdc134*^{-/-} mice (Fig. 2B), and no CCDC134 protein was detected with the use of a specific antibody to CCDC134 (Fig. 2C).

However, *Zp3-Cre-Ccdc134*^{+/-} mice appeared to be grossly normal. These heterozygotes bred without difficulty and delivered normal sized pups. No histologic deficits were observed. No apparent anatomic or microscopic features could reliably discriminate heterozygotes from their wild-type littermates. Previous study revealed that CCDC134 illustrated potent antitumor effects by augmenting CD8^{+} T-cell-mediated immunity (3), therefore different immune cell populations were analyzed in the spleen and thymus. The results indicated no obvious difference between heterozygotes and their

wild-type littermates. Additionally, B16 graft tumors were established in *Ccdc134*^{+/-} and *Ccdc134*^{+/+} controls, and it was demonstrated that *Ccdc134*^{+/-} mice may slightly accelerate tumor growth compared with wild-type controls; however, no significant difference was observed (data not shown). These data prompted us to restrict our efforts to the comparison of the wild-type and *Ccdc134*^{-/-} populations, to define rigorously the mutant phenotype without consideration of subtle or dose-dependent deficits.

Dynamic expression analyses of Ccdc134 in whole embryos during embryogenesis. To determine whether *Ccdc134* expression was altered at various developmental stages of the embryo, the mRNA expression level of *Ccdc134* at four developmental stages was compared. The expression level of *Ccdc134* decreased from E6.5 to E9.5, followed by an increasing trend from E9.5 to E12.5, and then a decrease at E14.5. Thus, *Ccdc134* mRNA showed the highest expression level at E12.5 (Fig. 3A).

To gain further insight into the spatial and temporal expression patterns of CCDC134 during embryonic development, whole mount embryo sections were analyzed by immunohistochemistry using specific rabbit anti-CCDC134 antibody. This revealed histological details of CCDC134 expression in the developing mouse embryo. At E6.5, the most prominent expression was observed in the Reichert's membrane and endoderm. Furthermore, CCDC134 expression was detected in the neural tube and trophoblastic giant cells at E9.5. With the development of the mouse embryo, prominent expression of CCDC134 was detected in the somite and major organs, including the liver and lung, from E12.5 to E14.5 (Fig. 3B). At these stages, CCDC134 was highly expressed in the somite and liver, suggesting that CCDC134 participated in the development and formation of major organs.

Morphological and histological pathology of Ccdc134^{-/-} *embryos.* To assess the role of CCDC134 throughout development, *Ccdc134*^{+/+}, *Ccdc134*^{+/-} and *Ccdc134*^{-/-} embryos were euthanized at E10.5-E16.5. Necropsies through this interval demonstrated that *Ccdc134*^{-/-} embryos appeared similar to *Ccdc134*^{+/+} and *Ccdc134*^{+/-} littermates at E10.5, while *Ccdc134*^{-/-} embryos exhibited severe hemorrhaging (100% penetrance) in the brain ventricular space and neural tube at E13.5. Additionally, *Ccdc134*^{-/-} embryos later than E13.5 looked anemic, and their size was slightly smaller than those of wild-type embryos (Fig. 4A). Subsequently, embryos at E16.5 were isolated, and the absorbed embryos with genotypes *Ccdc134*^{-/-} were noted. Thus, these data further suggest that *Ccdc134* deletion causes embryonic lethality. In addition, in contrast to *Ccdc134*^{+/+} and *Ccdc134*^{+/-} embryos whose red-brown livers invariably filled a large portion of the abdomen, the livers of *Ccdc134*^{-/-} embryos were considerably smaller (Fig. 4B). The total cell number per fetal liver was ~2×10^6 in *Ccdc134*^{+/+} livers and ~5×10^5 in *Ccdc134*^{-/-} livers, suggesting that *Ccdc134* deficiency affects the number of fetal liver cells and may lead to a defect in hematopoiesis (Fig. 4C).

Whole-mount histologic sections of *Ccdc134*^{-/-} embryos demonstrated liver abnormalities in later stage embryos. The fetal livers were markedly smaller and hypoplastic (Fig. 5A). Additionally, compared with their littermates, severe
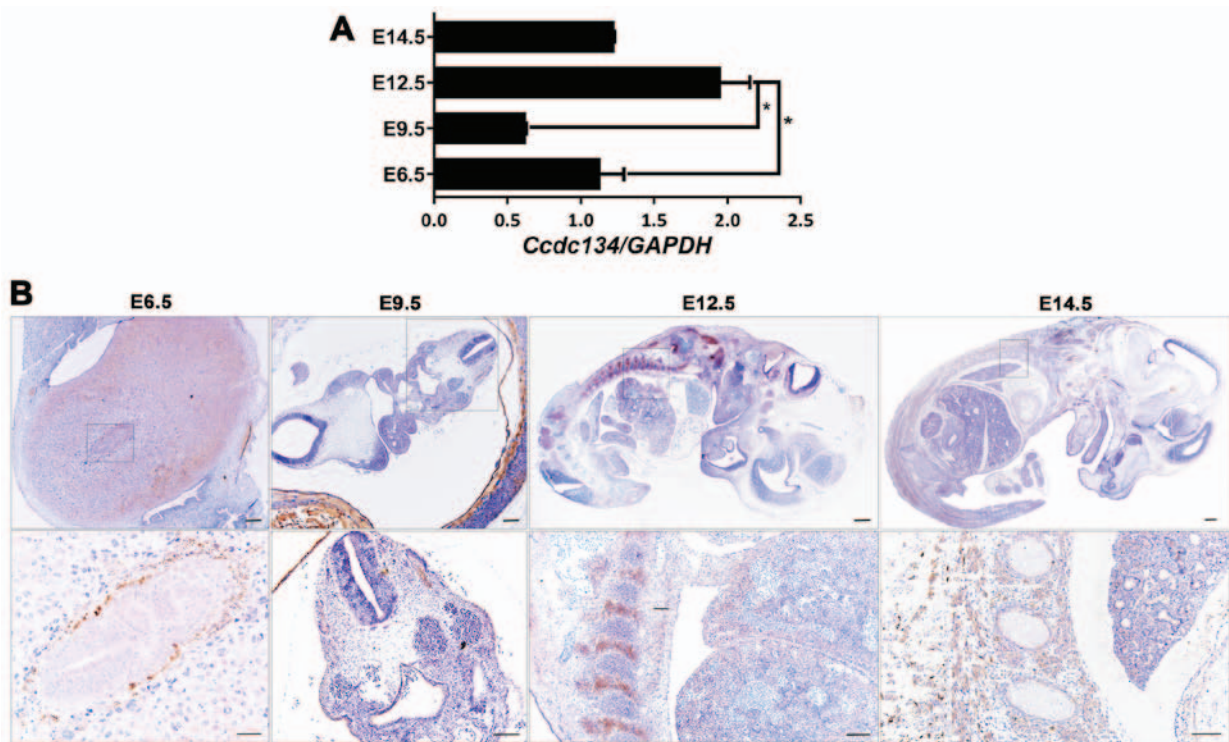
Figure 3. Spatiotemporal expression pattern of CCDC134 at four stages of mouse embryo development (E6.5, E9.5, E12.5 and E14.5). (A) Total RNA was obtained from mouse embryos. Reverse transcription-quantitative polymerase chain reaction data were normalized to the level of *GAPDH*. Data are presented as the mean ± standard deviation for each group of at least three embryos from different mothers. (B) Sagittal sections of embryos immunostained for CCDC134 protein. Higher magnification of the regions in the box is outlined (representative of three embryos). Scale bar, 100 μm. *P<0.05 as indicated. E, embryonic day; CCDC134, coiled-coil domain containing 134.

hemorrhage and overall brain disorganization was detected in the *Ccdc134*$^{-/-}$ embryo brain ventricular space (Fig. 5B). Concentric hypertrophy of the cardiac ventricular wall was also present in *Ccdc134*$^{-/-}$ embryos, suggesting increased vascular resistance (Fig. 5C). Furthermore, vasculature malformation was also noted, although blood cells present in *Ccdc134*$^{-/-}$ embryos appeared morphologically normal (Fig. 5D). However, the lungs of *Ccdc134*$^{-/-}$ embryos and littermate controls presented normal branching of the bronchioalveolar tree, with progressive thinning of the alveolocapillary membrane and flattening of the terminal sac epithelium (Fig. 5E). Structural changes in the placenta, leading to altered hemodynamics or surface area available for nutrient exchange, have been demonstrated to result in reductions in growth, heart defects and perinatal morbidity (14) (Fig. 5F). Given this, whether loss of *Ccdc134* altered the morphology of the placenta was investigated. The placenta of *Ccdc134*$^{-/-}$ embryos was thinner and poorly developed, and demonstrated a prominence of laby-rinth trophoblasts, which were arranged into poorly formed maternal vascular spaces; however, the thin-walled capillary bed of fetal circulation was ill defined (Fig. 5F).

Lethality due to reduced cell proliferation and vascular defects in Ccdc134$^{-/-}$ *embryos.* To clarify the causes of the liver abnormality in *Ccdc134*$^{-/-}$ embryos, immunohistochemical analysis was performed in transverse sections from *Ccdc134*$^{-/-}$ embryos at E13.5. As demonstrated in Fig. 6, CCDC134 expression was initially examined in vascular endothelial cells and some differentiated erythroid cells of fetal livers; however, *Ccdc134*$^{-/-}$ embryos were identified by immunostaining for the

absence of CCDC134 protein (Fig. 6A). As the embryonic liver is the main site of hematopoiesis in the second-half of murine gestation, it appeared that poor oxygenation secondary to anemia may contribute to embryonic demise (15). Erythroid cells of fetal livers were detected using the antibody against Ter119, which is a surface marker for differentiated erythroid cells (16). As demonstrated in Fig. 6A, no obvious difference was observed between the fetal liver of *Ccdc134*$^{-/-}$ embryos and wild-type embryos.

To further evaluate the existence of the vascular integrity defect, immunohistochemical analysis with specific antibody against Vegfr-2 was conducted, which is a type V receptor tyro-sine kinase, predominantly known to be expressed in vascular endothelial cells (17). The representative example of Fig. 6A illustrates a discontinuous Vegfr-2-positive endothelial cell barrier in fetal livers in *Ccdc134*$^{-/-}$ embryos compared with *Ccdc134*$^{+/+}$ and *Ccdc134*$^{+/-}$ embryos, which may contribute to fetal liver abnormality. In order to further investigate the influ-ence of *Ccdc134* deficiency on cell proliferation in fetal livers, a proliferation study was performed at E13.5. Ki-67 immunos-taining detection of cycling cells revealed a significant decrease of Ki-67^{+} nuclei in fetal livers of *Ccdc134*$^{-/-}$ embryos compared with wild-type embryos (Fig. 6A and C). Observations of *Ccdc134*$^{-/-}$ embryos support that the phenotype of an abnormal fetal liver described at E13.5 above is due to a significant decrease in proliferation and impaired blood vessels.

Gross morphology suggested severe hemorrhage in the brain ventricular space of *Ccdc134*$^{-/-}$ embryos at E13.5. Vascular integrity defect was further analyzed with anti-Vegfr-2 anti-body. As demonstrated in Fig. 6B, Vegfr-2 was expressed by
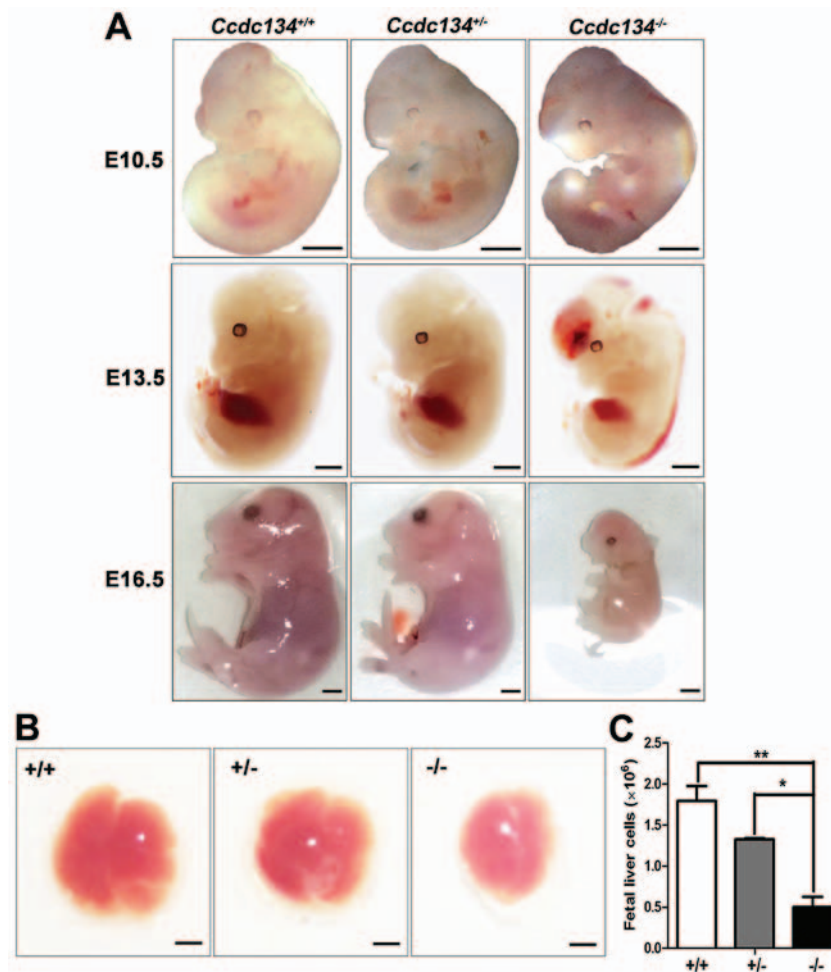
Figure 4. Gross appearance of *Ccdc134*^{+/+}, *Ccdc134*^{+/-} and *Ccdc134*^{-/-} mouse embryos and fetal livers. Embryos were analyzed from at least three separate experiments. (A) Representative phenotypes of E10.5, E13.5 and E16.5 embryos with genotypes *Ccdc134*^{+/+}, *Ccdc134*^{+/-} and *Ccdc134*^{-/-} (littermate controls). Scale bar, 200 μm. (B) Representative E13.5 fetal livers from *Ccdc134*^{+/+}, *Ccdc134*^{+/-} and *Ccdc134*^{-/-} embryos. Scale bar, 100 μm. (C) Quantitative analysis of cell number in E13.5 fetal livers (representative of three replicates). Data are presented as the mean ± standard deviation for each group of at least three embryos from different mothers. *P<0.05 and **P<0.01 as indicated. CCDC134, coiled-coil domain containing 134.

both cerebral tissue and vessels in the forebrain, midbrain and hindbrain of embryos at E13.5; however, compared with the *Ccdc134*^{+/+} and *Ccdc134*^{+/-} embryos, overall brain disorganization in the *Ccdc134*^{-/-} embryo was observed. Additionally, a significant reduction of vascular density was observed in the *Ccdc134*^{-/-} embryos compared with their littermates (Fig. 6D). Taken together, these findings suggest that *Ccdc134* may be associated with angiogenesis.

Discussion

The present study reported the generation of complete *Ccdc134* null mice by deleting the four coding exons of *Ccdc134* using a Cre-loxP system, which abolishes the expression of CCDC134 protein. The present study also demonstrated the CCDC134 expression pattern during embryogenesis. Furthermore, a large number of postnatal mice were examined and no homozygous *Ccdc134* KO mice were identified, suggesting that complete loss of *Ccdc134* resulted in embryonic lethality.

The main processes involved in mouse embryonic development include regional specification, morphogenesis, cell differentiation, cell growth and the overall control of timing (18). We speculate that the main cause of mortality in *Ccdc134*^{-/-} embryos

at E13.5 was anemia, as severe hemorrhage in the brain and neural tube was identified. Notably, mortality at this age corresponds to a developmental period during which defects of the heart or placenta often lead to embryonic lethality (19). Additionally, the placentas of *Ccdc134*^{-/-} embryos were thinner and poorly developed and showed a prominence of labyrinth trophoblasts. The cell numbers in *Ccdc134*^{-/-} fetal livers were significantly reduced compared with the number in wild-type livers. Also, fewer Vegfr-2-positive endothelial cells and reduced cell proliferation were demonstrated in fetal livers of *Ccdc134*^{-/-} embryos compared to that of wild-type embryos. It is also interesting to note that *Ccdc134*^{-/-} embryos demonstrated broad areas of extravasated blood associated with discontinuous and defective blood vessels. Angiogenesis is important in embryonic development, in which endothelial progenitor cells (EPCs) serve critical roles (20). Furthermore, angiogenesis is driven by newly formed EPCs migrating from the sites of hematopoietic stem cell (HSC) development (21). Bone marrow begins to function as a source of HSCs just before birth, whereas in embryogenesis, multi-lineage hematopoietic progenitors exist in the extraembryonic yolk sac at E8.25, and in the placenta and embryonic aorta-gonad-mesonephros region at E10 (22). From E12 to birth, the fetal liver is the main site for definitive HSC formation (23).
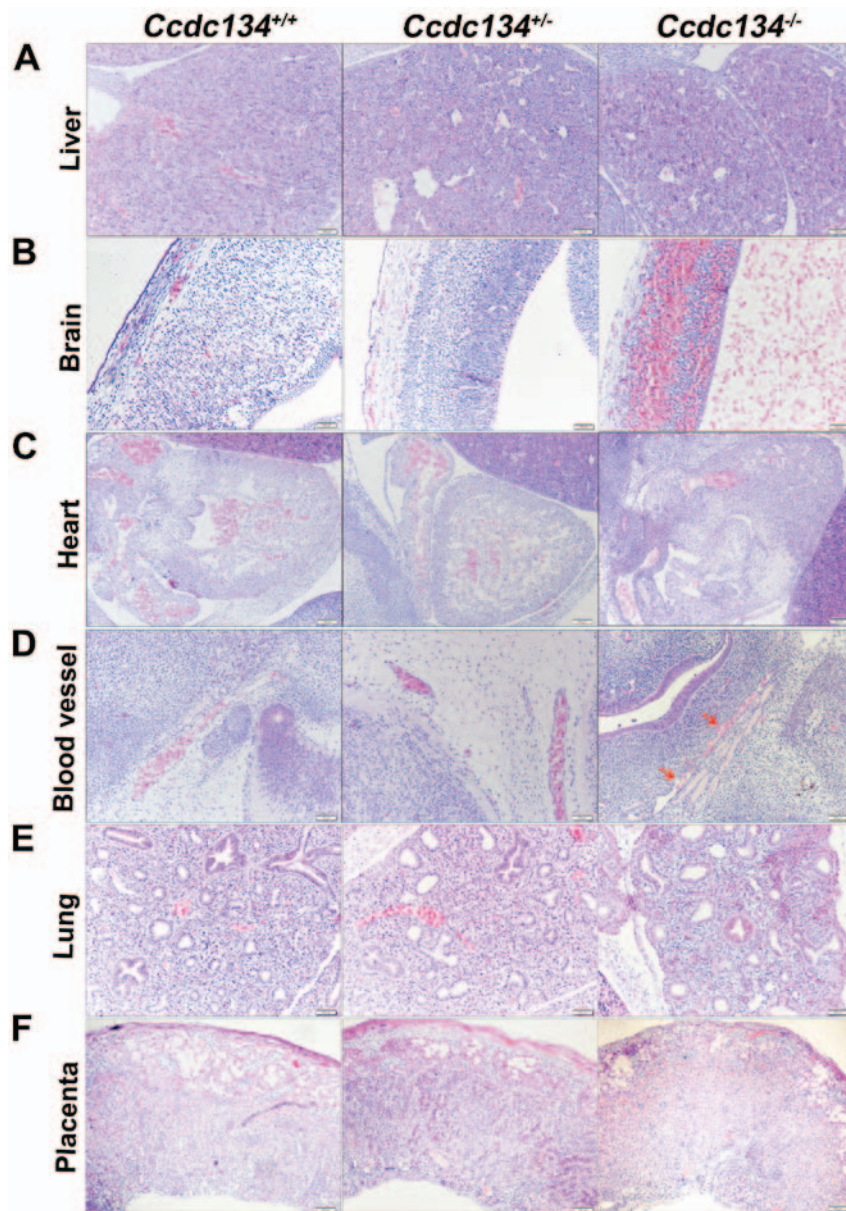
Figure 5. Histopathology of *Ccdc134⁻/⁻* embryos compared with *Ccdc134⁺/⁺* and *Ccdc134⁺/⁻* littermates at embryonic day 13.5. Hematoxylin and eosin-stained sections of (A) liver, (B) brain, (C) heart, (D) blood vessel, (E) lung and (F) placenta (representative of three replicates). Red arrow indicates discontinuous blood vessel walls. Scale bar, 100 *µm*. *Ccdc134*, coiled-coil domain containing 134.

These findings implied that *Ccdc134* may have a role in hematopoiesis and angiogenesis during embryonic development. Therefore, conditional deletion of *Ccdc134* in hematopoietic stem cells (Vav-Cre) and endothelial cells (Tie2-Cre) may be utilized to further investigate the function of CCDC134 in the differentiation of HSCs and angiogenesis.

In conjunction with our previous results (4), CCDC134 was identified to be a novel partner of hADA2a protein, which was a core component of the yeast alteration/deficiency in activation (ADA)/GCN5 HAT complexes to facilitate the acetylation of nucleosomal histones (24). Additionally, CCDC134 may act as a critical regulator of hADA2a stability and activity, and participate in the PCAF complex via hADA2a to affect its HAT activity, which acetylates H3K14 and H4K8 (24). Deletion of GCN5 and PCAF resulted in embryo lethality between E9.5 and E11.5, indicating that PCAF and GCN5 served important roles in embryogenesis (25). Also, GCN5 and PCAF had redundant functions in mouse embryonic fibroblasts (26). Additionally, HAT PCAF/lysine acetyltransferase 2B was an important factor of the Hedgehog signaling pathway that served an important role in embryonic patterning and development of various tissues and organs, as well as in maintaining and repairing mature tissues in adults (27). During embryogenesis, the early mammalian embryo was characterized by large-scale chromatin remodeling, including changes in histone variant incorporation, global changes in DNA, and histone tail modification (28,29). Histone H3 acetylation in the nucleosome core occurred with different temporal kinetics during mouse pre-implantation development, and further affected embryo development (30). In addition, various studies have demonstrated that angiogenesis is precisely regulated by soluble growth factors and receptor-mediated signals. Vegfr-2 is a key regulator of angiogenesis, and its expression and function are regulated by acetylation under dynamic control of the acetyltransferase p300 (31,32).
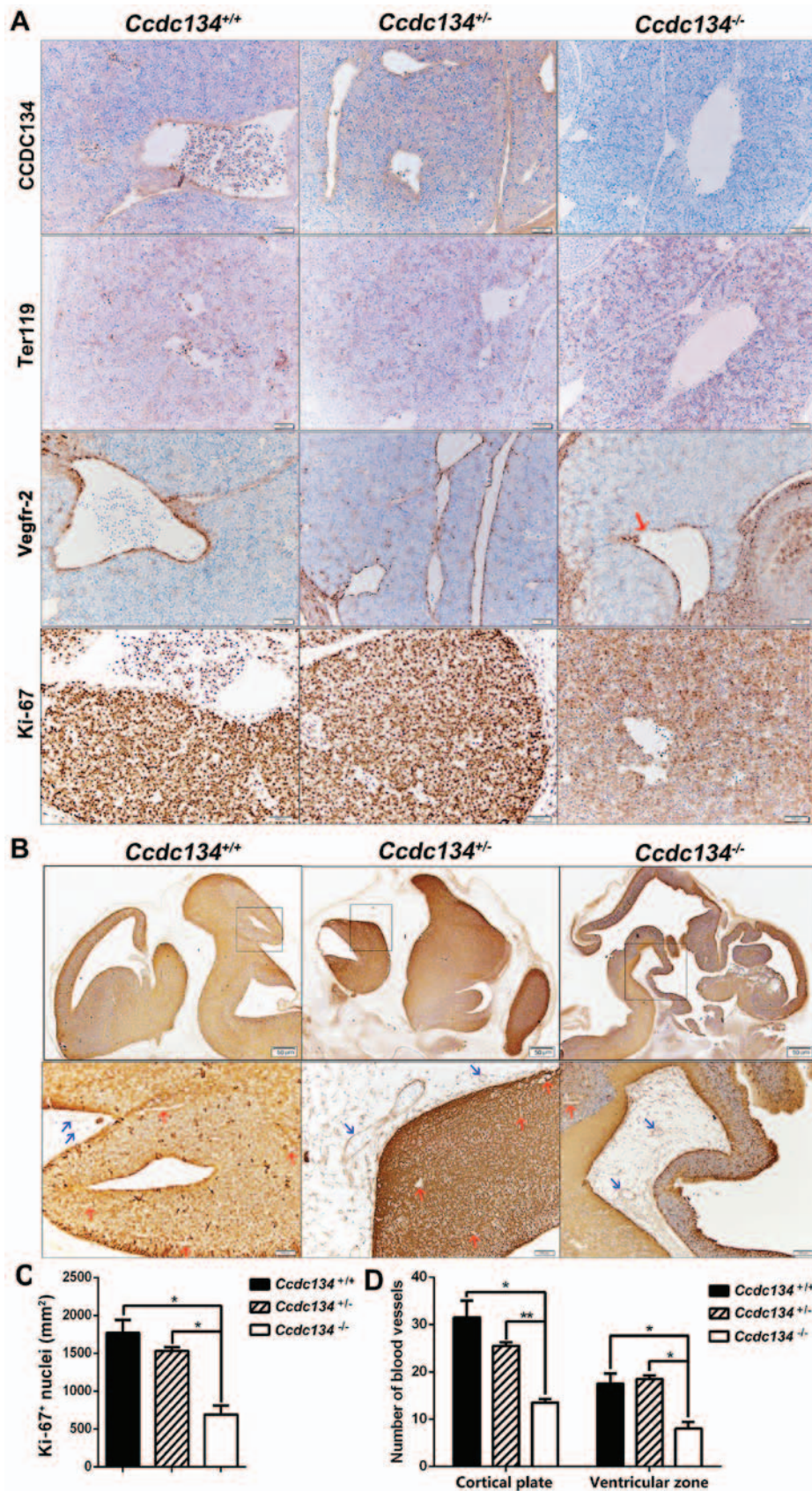
Figure 6. Histological phenotypes of *Ccdc134*⁻/⁻ embryos at embryonic day 13.5 compared with *Ccdc134*⁺/⁺ and *Ccdc134*⁺/⁻ littermates. (A) The serial sections of fetal livers were used for staining with different antibodies, including rabbit anti-CCDC134 antibody to identify CCDC134 deletion, anti-Vegfr-2 antibody for identifying vascular endothelial cells, anti-Ter119 antibody to detect erythroid cells and anti-Ki-67 to detect proliferative cells. Red arrow indicates discontinuous blood vessel walls. Scale bar, 100 μm. (B) Serial sections of fetal brains were stained with anti-Vegfr-2 antibody. Higher magnification views (shown in the boxes) illustrate the presence of blood vessels in the cortical plate (red arrow) and ventricular zone (blue arrow). Scale bars, 50 or 100 μm. Images are representative of two independent experiments. (C) Quantitative analysis of Ki-67⁺ cells from five randomly selected fields in fetal livers. (D) Quantification of blood vessel number based on Vegfr-2 staining from five randomly selected fields in the fetal brain. Data are presented as the mean ± standard deviation for each group of three embryos. *P<0.05 and **P<0.01 as indicated. Vegfr-2, vascular endothelial growth factor receptor-2; CCDC134, coiled-coil domain containing 134.

Furthermore, PCAF acts as a master switch in the inflammatory processes required for effective arteriogenesis (33). Therefore, the cause of embryonic mortality in the present study may be due to defective hematopoiesis and angiogenesis, which likely cause mortality due to failure of acetylation modification of key regulators during embryo development.

In conclusion, the present results support the conclusion that disruption of *Ccdc134* expression in mice leads to embryonic lethality. In addition, the present preliminary studies suggested that *Ccdc134* may be related to hematopoiesis and angiogenesis, and further studies will be performed. Thus, the *Ccdc134* null line provides a critical tool for determining the physiological roles of *Ccdc134*. Furthermore, *Ccdc134^{fl/fl}* mice will be important for the analysis of *Ccdc134* function in specific cell types and the extension into analysis of *Ccdc134* loss of function in adult animals.

Acknowledgements

References

1. Huang J, Shi T, Ma T, Zhang Y, Ma X, Lu Y, Song Q, Liu W, Ma D and Qiu X: CCDC134, a novel secretory protein, inhibits activation of ERK and JNK, but not p38 MAPK. Cell Mol Life Sci 65: 338-349, 2008.
2. Zhong J, Zhao M, Luo Q, Ma Y, Liu J, Wang J, Yang M, Yuan X, Sang J and Huang C: CCDC134 is down-regulated in gastric cancer and its silencing promotes cell migration and invasion of GES-1 and AGS cells via the MAPK pathway. Mol Cell Biochem 372: 1-8, 2013.
3. Huang J, Xiao L, Gong X, Shao W, Yin Y, Liao Q, Meng Y, Zhang Y, Ma D and Qiu X: Cytokine-like molecule CCDC134 contributes to CD8⁺ T-cell effector functions in cancer immunotherapy. Cancer Res 74: 5734-5745, 2014.
4. Huang J, Zhang L, Liu W, Liao Q, Shi T, Xiao L, Hu F and Qiu X: CCDC134 interacts with hADA2a and functions as a regulator of hADA2a in acetyltransferase activity, DNA damage-induced apoptosis and cell cycle arrest. Histochem Cell Biol 138: 41-55, 2012.
5. Schiltz RL, Mizzen CA, Vassilev A, Cook RG, Allis CD and Nakatani Y: Overlapping but distinct patterns of histone acetylation by the human coactivators p300 and PCAF within nucleosomal substrates. J Biol Chem 274: 1189-1192, 1999.
6. Garlanda C, Dinarello CA and Mantovani A: The interleukin-1 family: Back to the future. Immunity 39: 1003-1018, 2013.
7. Yang H, Wang H, Chavan SS and Andersson U: High mobility group box protein 1 (HMGB1): The prototypical endogenous danger molecule. Mol Med 21 (Suppl 1): S6-S12, 2015.
8. Li G, Xu C, Lin X, Qu L, Xia D, Hongdu B, Xia Y, Wang X, Lou Y, He Q, *et al*: Deletion of Pdcd5 in mice led to the deficiency of placenta development and embryonic lethality. Cell Death Dis 8: e2811, 2017.
9. Livak KJ and Schmittgen TD: Analysis of relative gene expression data using real-time quantitative PCR and the 2(-ΔΔC(T)) method. Methods 25: 402-408, 2001.
10. Farley FW, Soriano P, Steffen LS and Dymecki SM: Widespread recombinase expression using FLPeR (flipper) mice. Genesis 28: 106-110, 2000.
11. Rodríguez CI, Buchholz F, Galloway J, Sequerra R, Kasper J, Ayala R, Stewart AF and Dymecki SM: High-efficiency deleter mice show that FLPe is an alternative to Cre-loxP. Nat Genet 25: 139-140, 2000.
12. Lewandoski M, Meyers EN and Martin GR: Analysis of Fgf8 gene function in vertebrate development. Cold Spring Harb Symp Quant Biol 62: 159-168, 1997.
13. de Vries WN, Binns LT, Fancher KS, Dean J, Moore R, Kemler R and Knowles BB: Expression of Cre recombinase in mouse oocytes: A means to study maternal effect genes. Genesis 26: 110-112, 2000.
14. Renaud SJ, Karim Rumi MA and Soares MJ: Review: Genetic manipulation of the rodent placenta. Placenta 32 (Suppl 2): S130-S135, 2011.
15. Dzierzak E, Medvinsky A and de Bruijn M: Qualitative and quantitative aspects of haematopoietic cell development in the mammalian embryo. Immunol Today 19: 228-236, 1998.
16. Koulnis M, Pop R, Porpiglia E, Shearstone JR, Hidalgo D and Socolovsky M: Identification and analysis of mouse erythroid progenitors using the CD71/TER119 flow-cytometric assay. J Vis Exp 54: e2809, 2011.
17. Breier G, Clauss M and Risau W: Coordinate expression of vascular endothelial growth factor receptor-1 (flt-1) and its ligand suggests a paracrine regulation of murine vascular development. Dev Dyn 204: 228-239, 1995.
18. Slack JM: Essential Developmental Biology. 3rd edition. Wiley-Blackwell, Oxford, 2012.
19. Savolainen SM, Foley JF and Elmore SA: Histology atlas of the developing mouse heart with emphasis on E11.5 to E18.5. Toxicol Pathol 37: 395-414, 2009.
20. Folkman J: Angiogenesis in cancer, vascular, rheumatoid and other disease. Nat Med 1: 27-31, 1995.
21. Smith AG: Embryo-derived stem cells: Of mice and men. Annu Rev Cell Dev Biol 17: 435-462, 2001.
22. Coşkun S, Chao H, Vasavada H, Heydari K, Gonzales N, Zhou X, de Crombrugghe B and Hirschi KK: Development of the fetal bone marrow niche and regulation of HSC quiescence and homing ability by emerging osteolineage cells. Cell Rep 9: 581-590, 2014.
23. Golub R and Cumano A: Embryonic hematopoiesis. Blood Cells Mol Dis 51: 226-231, 2013.
24. Grant PA, Duggan L, Côté J, Roberts SM, Brownell JE, Candau R, Ohba R, Owen-Hughes T, Allis CD, Winston F, *et al*: Yeast Gcn5 functions in two multisubunit complexes to acetylate nucleosomal histones: Characterization of an Ada complex and the SAGA (Spt/Ada) complex. Genes Dev 11: 1640-1650, 1997.
25. Yamauchi T, Yamauchi J, Kuwata T, Tamura T, Yamashita T, Bae N, Westphal H, Ozato K and Nakatani Y: Distinct but overlapping roles of histone acetylase PCAF and of the closely related PCAF-B/GCN5 in mouse embryogenesis. Proc Natl Acad Sci USA 97: 11303-11306, 2000.
26. Jin Q, Yu LR, Wang L, Zhang Z, Kasper LH, Lee JE, Wang C, Brindle PK, Dent SY and Ge K: Distinct roles of GCN5/PCAF-mediated H3K9ac and CBP/p300-mediated H3K18/27ac in nuclear receptor transactivation. EMBO J 30: 249-262, 2011.
27. Malatesta M, Steinhauer C, Mohammad F, Pandey DP, Squatrito M and Helin K: Histone acetyltransferase PCAF is required for Hedgehog-Gli-dependent transcription and cancer cell proliferation. Cancer Res 73: 6323-6333, 2013.
28. Hemberger M, Dean W and Reik W: Epigenetic dynamics of stem cells and cell lineage commitment: Digging Waddington's canal. Nat Rev Mol Cell Biol 10: 526-537, 2009.
29. Burton A and Torres-Padilla ME: Chromatin dynamics in the regulation of cell fate allocation during early embryogenesis. Nat Rev Mol Cell Biol 15: 723-734, 2014.
30. Ziegler-Birling C, Daujat S, Schneider R and Torres-Padilla ME: Dynamics of histone H3 acetylation in the nucleosome core during mouse pre-implantation development. Epigenetics 11: 553-562, 2016.
31. Rahimi N and Costello CE: Emerging roles of post-translational modifications in signal transduction and angiogenesis. Proteomics 15: 300-309, 2015.
32. Zecchin A, Pattarini L, Gutierrez MI, Mano M, Mai A, Valente S, Myers MP, Pantano S and Giacca M: Reversible acetylation regulates vascular endothelial growth factor receptor-2 activity. J Mol Cell Biol 6: 116-127, 2014.
33. Bastiaansen AJ, Ewing MM, de Boer HC, van der Pouw Kraan TC, de Vries MR, Peters EA, Welten SM, Arens R, Moore SM, Faber JE, *et al*: Lysine acetyltransferase PCAF is a key regulator of arteriogenesis. Arterioscler Thromb Vasc Biol 33: 1902-1910, 2013.